chemosensors

MDPI

Article

A Peptide-Based Trap for Metal Ions Studied by Electron Paramagnetic Resonance

Victoria N. Syryamina [1], Alvaro S. Siano [2], Fernando Formaggio [3] and Marta De Zotti [3,4,*]

[1] Voevodsky Institute of Chemical Kinetics and Combustion, RAS, 630090 Novosibirsk, Russia; v_syryamina@kinetics.nsc.ru
[2] Departamento de Química Organica, Facultad de Bioquímica y Ciencias Biologicas (FBCB), Universidad Nacional del Litoral (UNL), 3000 Santa Fe, Argentina; alvarosiano@gmail.com
[3] Padova Unit, CNR Institute of Biomolecular Chemistry, University of Padova, 35131 Padova, Italy; fernando.formaggio@unipd.it
[4] Centro Interdipartimentale di Ricerca "Centro Studi di Economia e Tecnica dell'energia Giorgio Levi Cases", 35131 Padova, Italy
* Correspondence: marta.dezotti@unipd.it; Tel.: +39-0498275280

Abstract: Peptide-based materials provide a versatile platform for sensing and ion sequestration since peptides are endowed with stimuli-responsive properties. The mechanism of molecular sensing is often based on peptide structural changes (or switching), caused by the binding of the target molecule. One scope of sensing applications is the selection of a specific analyte, which may be achieved by adjusting the structure of the peptide binding site. Therefore, exact knowledge of peptide properties and 3D-structure in the 'switched' state is desirable for tuning the detection and for further molecular construction. Hence, here we demonstrate the performance of Electron Paramagnetic Resonance (EPR) spectroscopy in the identification of metal ion binding by the antimicrobial peptide trichogin GA IV. Na(I), Ca(II), and Cu(II) ions were probed as analytes to evaluate the impact of coordination number, ionic radii, and charge. Conclusions drawn by EPR are in line with literature data, where other spectroscopic techniques were exploited to study peptide-ion interactions for trichogin GA IV, and the structural switch from an extended helix to a hairpin structure, wrapped around the metal ion upon binding of divalent cations was proposed.

Keywords: peptide; metal ions; chelation; conformational changes; trichogin GA IV; EPR/ESR

Citation: Syryamina, V.N.; Siano, A.S.; Formaggio, F.; De Zotti, M. A Peptide-Based Trap for Metal Ions Studied by Electron Paramagnetic Resonance. *Chemosensors* **2022**, *10*, 71. https://doi.org/10.3390/chemosensors10020071

Academic Editors: Krzysztof Żamojć, Joanna Makowska and Dariusz Wyrzykowski

Received: 14 December 2021
Accepted: 7 February 2022
Published: 10 February 2022

1. Introduction

Peptides attract attention not only for their antibiotic activity [1–3] but also for applications in nanotechnology, as molecular sensors or logical elements, or as biomaterials for purifying water from environmental toxins [4–8]. Peptides are often able to provide a selective response to external stimuli, such as the presence of a specific analyte [9–17]. One of the most common reactions of peptides to an external stimulus is to undergo a conformational change that might be reversible [18–20]. The activation can be triggered by a non-covalent interaction between the analyte and the peptide binding site or induced by temperature or pressure variation or light [21–25]. When a peptide is exploited in a smart biodevice, a clear knowledge of its physicochemical parameters and 3D structure in the 'switched on/off' states is therefore required. The molecular structure of the binding site and stability of its 'on/off' states can thus be fine-tuned, resulting in the production of biosensors with high selectivity to a specific analyte [26,27], or of bi-/multi-modal logical elements [28]. The prediction of the conformational changes occurring when the peptide switches between the 'on/off' states is relevant for detection, and to produce materials with a specific shape, size, or polydispersity [29], while the study of conformational stability is crucial for their application. In summary, the development, rational optimization, and implementation of smart materials require robust structural characterization of the

molecules used. For peptides, where so many factors affect the binding efficiency (peptide primary and secondary structures, solvent, pH, analyte nature), and the binding process could have several pathways, a reliable and robust way of experimental investigation is especially required.

The characterization at the molecular level is typically performed by several techniques: 2D NMR, circular dichroism, and X-ray diffraction for probing peptide helicity; FRET for identifying the analyte binding and for estimating the structural changes in the recipient; molecular dynamic and DFT calculations for predicting the binding site, to be compared with experimental data; microscopies for characterizing peptide supramolecular organizations, fluorescence spectroscopy for studying peptide-ion binding and revealing the complex structure, isothermal titration calorimetry, mass spectrometry, as well as other methods [7,19,22,24,30–35].

Besides the above-mentioned techniques, pulse dipolar Electron Paramagnetic Resonance spectroscopy (PDS EPR) [36–39] allows to obtain distance distribution functions between paramagnetic centers, naturally present in the system or artificially introduced via spin-labeling [40–42]. EPR is widely used for characterizing the conformation of peptides and proteins. When the secondary structure of a peptide is perturbed by analyte binding, EPR is not only a tool for monitoring the interaction between peptide and analytes, but also gives information about the flexibility (or stability) of such a complex, and about possible oligomerization or peptide aggregation [25,43,44]. It should be noted that, depending on the character of the binding (for example, the binding of metal ions through the main peptide chain is usually less selective and less efficient than through side chains [6]) and on the changes in the local peptide structure, the variation of the distance distribution function between labels can be subtle [45–47]. In this connection, the so-called rigid or semi-rigid labels, such as the nitroxide-bearing, C^{α}-tetrasubstituted residue TOAC (2,2,6,6-tetramethylpiperidine-1-oxyl-4-amino-4-carboxylic acid, Figure 1) possess a clear advantage in comparison with the typically used spin labels with flexible linkers [42,48]. Indeed, when inserted in the peptide sequence, those rigid labels become reliable probes of any conformational change.

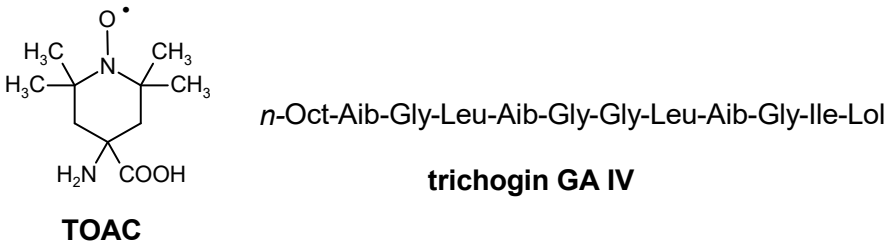

Figure 1. Molecular structure of TOAC and amino acid sequence of trichogin GA IV (*n*-Oct, octanoyl; Aib, α-aminoisobutyric acid; Lol, leucinol).

Here, we demonstrate the effectiveness of EPR spectroscopy in characterizing structural changes on the double TOAC-labeled peptide analog of the helical undecapeptide trichogin GA IV (Figure 1) upon binding metal cations.

TOAC can replace Aib in the trichogin native sequence since it has the same ability to induce helical structures. Despite the relatively short length, trichogin and its analogs have already been demonstrated to act as ion traps, with a selective binding affinity. Previous studies published in the literature highlighted that, while multivalent, transition and rare-earth metal ions [Ca(II), Gd(III), and Tb(III)] are able to bind to trichogin, no binding was observed for monovalent alkaline ions [Na(I) and K(I)] [33,34]. Trichogin does not contain amino acid residues known to interact with cations (such as cysteine, histidine, serine, or aspartic and glutamic acids). In the literature, on the basis of conformational studies (by circular dichroism, 2D-NMR, X-ray diffraction analysis), it was suggested that a pivotal role in analyte binding is played by the central, flexible -Gly^5-Gly^6- motif of trichogin [49], which may form a loop around the metal ion, combined with the relatively short length of

trichogin (ca. 2.2 nm in a 3_{10}-helix [24,44]). These features may provide either a structural match for the coordination shell of the metal ion or the right coordination number for specific ions. To shed light on peptide–ion interaction, we tested several analytes with different binding affinities to the peptide: Na(I) as a non-reacting analyte, Ca(II) as a binding analyte [33], and Cu(II) as one of the most convenient EPR-active ions.

2. Materials and Methods

2.1. Peptide Synthesis and Sample Preparation

The double spin-labeled analog of trichogin GA IV Tri^{1,8} [24] was produced in good yield by solid-phase peptide synthesis, following a published procedure [50,51]:

*n*Oct-**TOAC^{1}**-Gly-Leu-Aib-Gly-Gly-Leu-**TOAC^{8}**-Gly-Ile-Leu-Lol, **Tri^{1,8}**

The peptide and each of the tested salts (NaCl, $CaCl_2$, or $CuCl_2$) were co-dissolved in ethanol; 5% methanol (*v*/*v*) was added for glass formation (alcohols were obtained from Ekros-Analytics, St. Petersburg, Russian Federation). Solutions at a peptide concentration of 0.2 mM were prepared. The peptide-to-metal ion ratio was 1:1 for all tested cations, plus 1:2, 2:1 for Na(I) and Ca(II) ions. The solutions were placed in EPR tubes with 2.9 mm o.d. The solution height in the tube was kept below 4 mm. The samples formed a transparent glass after shock-freezing in liquid nitrogen. Peptide without metal ions and the systems at peptide-to-metal ion ratio 1:1 were analyzed in duplicate.

2.2. EPR Measurements

Continuous wave (CW) and pulse X-band EPR spectra were acquired using a Bruker Elexsys E580 spectrometer equipped with a cylindrical resonator with a shaped dielectric inset [52]. CW EPR measurements were performed both at room temperature (RT) and at 100 K. At 100 K, the microwave (mw) power was attenuated to −45 and −25 dB when measuring nitroxides and Cu(II) species, respectively, to avoid spectra saturation; at room temperature, the mw power was attenuated to −35 and −25 dB for nitroxides and Cu(II) species, respectively. The calibrated, non-attenuated output mw power of the Gunn diode was 200 mW. The modulation frequency was set to 100 kHz. The modulation amplitude was set to 0.05 mT or 0.5 mT to detect nitroxides or Cu(II), respectively. The sweep width was 15 mT for nitroxides and 150 mT for the Cu(II) species. A time constant of 20.48 ms and a conversion time of 40.96 ms were used.

Experiments below room temperature were carried out with a helium flow cryostat (ER 4118 CF, Oxford Instruments) for adjusting and stabilizing the measurement temperature. Pulse EPR experiments were acquired at 70 K using liquid nitrogen and cryostat pumping.

The 3-pulse DEER measurements were performed by pulse sequence $t_{pulse} - T - t_{pump} - (\tau - T) - t_{pulse} - \tau - echo$, the length of mw pulses was set to t_{pulse} = 16 ns, the length of pumping pulse was set to t_{pump} = 20 ns, the mw power was adjusted to obtain the maximal echo signal. The time delay T for the pumping pulse was initially set to 200 ns before the first registration pulse and then scanned with a 4 ns sampling step. The pumping ν_B frequency was chosen to the maximum of the echo-detected EPR spectrum; the frequency offset was chosen symmetrically with respect to the resonator dip, $\nu_A - \nu_B$ = 70 MHz. The mw power of the pumping pulse was adjusted by nutation measurements at $\nu_A = \nu_B$. The time delay τ was set to 1000 ns, the sequence repetition time was kept at 1 ms, providing more than 90% of echo intensity. The minimal reliable r_{min} value was limited by the sampling frequency [53] and by the amplitude of the pumping pulse [54] to 1.57 nm under the chosen experimental conditions. The phase jumps due to the passage of the pumping pulse through the first detection pulse were eliminated by the measuring scheme described by Milov [55]. Each DEER measurement was repeated several times to access an overall SNR value of 100, and the average DEER trace was used for further analysis.

The chosen experimental setup (measuring temperature, length of the dipolar trace, sampling frequency, and length of the pumping pulse) is in line with the recommended conditions to extract the distance distribution function within the range 1.57–2.9 nm [56–58].

2.3. Data Processing and Analysis

CW EPR spectra were background corrected and normalized to the double integral. The spectra simulations were performed by EasySpin software [59].

The modulation of the electron spin echo signal by dipolar coupling is the result of independent contributions by intra- ($V_{intra}(T)$) and inter-molecular ($V_{inter}(T)$), or background, spin–spin interactions. Thus, first of all, DEER traces were background-corrected by stretched exponential function $exp(-(kT)^{d/3})$. Normalized dipolar trace $V_n(T)$ was then obtained for the intra-molecular term as:

$$V_n(T) = \frac{V_{intra}(T) - V_{intra}(\infty)}{1 - V_{intra}(\infty)},$$

where $V_{intra}(\infty)$ is the intramolecular modulation depth, determined at an infinite time. Finally, the cosine Fourier transformation was performed on $V_n(T)$.

The multi-Gaussian (3-Gaussian) Monte Carlo simulation [60] was performed by means of a home-written script, for evaluation of the spin–spin distance distribution function. To avoid misinterpretation of the residual ^{1}H ESEEM from protons in the peptide structure and the solvation shell, distances below 1.54 nm (the magnetic field for the detection position being about 335 mT) were forbidden for the Monte Carlo sampling. The Gaussian simulation is the simplest model-based approach, independently used, and implemented in different software [57,60–63]. The consistency of the multi-Gaussian Monte Carlo simulations with the model-free Tikhonov-based approach [43] has previously been demonstrated [60,64,65]. The conformational changes undergone by trichogin are subtle: to confirm our results, we used also the DeerAnalysis software (version 2018) [62]. The background-corrected traces were analyzed by a model-free Tikhonov method; the regularization parameter was chosen at the maximum positive curvature region of the L-curve. The evaluated distance distribution functions were fitted by a Gaussian function for comparison with the results of the Monte Carlo simulations. The uncertainty of the mean TOAC-TOAC distances and the variance of the distance distribution was estimated by scanning the χ^2-surface, assuming the unimodal Gaussian distribution for the Monte Carlo approach [57], combined with the validation of the experimental data by the DeerAnalysis software [66]. Noise propagation in the distance domain was estimated from 1000 overall trials, using the following range of parameters and boundaries for validation: the white noise amplitude was varied by 1–1.5 times the original noise value; the dimension of background function was varied in the range from 3 to 3.1 (3.15). The upper limit was determined by simultaneous optimization in DeerAnalysis of both the d value and the background correction area, and it changes slightly among different samples; the starting point for background correction was varied within the interval of 100–120 ns. For comparison, the integral of each $f(r)$ curve was normalized to the unit. Small differences in distance distribution widths may arise from data regularization in the model-free approach [62], or the setup lower limit in the Monte Carlo algorithm.

3. Results and Discussion

3.1. Theoretical Background of the EPR Spectroscopy

The EPR spectrum is determined by the energy levels diagram of the unpaired electron(s), described by the spin Hamiltonian, which includes the electron and nuclear Zeeman (EZ and NZ) interactions, the electron–nuclear (e-n or hyperfine) interaction (HFI), and the electron–electron dipole–dipole (e-e d-d or dipolar) interaction:

$$H = \mu_B \sum_i \vec{B_0} g_i \vec{S_i} - \sum_i \mu_{in} B_0 g_{in} I_{i,z} + \sum_{i,j} \vec{S_i} A_{ij} \vec{I_j} + \sum_{i \neq j} \vec{S_i} D_{ij} \vec{S_j}, \quad (1)$$

where μ_B and μ_n are the Bohr and nuclear magnetons, B_0 is the static magnetic field, **g** are electron g-tensors, g_n the nuclear g value, S and I are the electron and nuclear spin operators, **A** is a HFI tensors, and **D** is a tensor of e-e d-d interaction. EPR spectra of

both nitroxide spin labels and copper spin probes are dominated by the EZ and NZ terms, resulting in a three-component spectrum for nitroxides (^{14}N, $I = 1$), and a quartet for copper species ($^{63/65}$Cu(II), $I = 3/2$). The hyperfine spectrum structure is further determined by weak couplings of the unpaired electron with local nuclear surrounding (HFI term) and other paramagnetic centers (e-e d-d term). Typically, in the absence of exchange coupling (i.e., when spin–spin distances are above 1.5 nm, and without hyperconjugation of the spin systems), the dipolar term is of about 1–13 MHz and usually masked under inhomogeneous line broadening.

When the paramagnetic metal ion is bound to the peptide, the local surroundings of both the metal ion and the peptide are perturbed, which in turn could modify the energy diagram, and affect the g-, HFI-, and dipolar tensors [25,45,67–69]. For EPR-silent metal ions in which ion-peptide binding induces structural changes in the peptide, probing distances between specific positions in the peptide allow monitoring of the interaction.

If structural changes in the TOAC-labeled peptide are significant, or the coordination shell of the paramagnetic metal ion changes significantly, the information upon binding of the ion can be detected by continuous wave (cw) EPR spectroscopy.

On the other hand, pulse EPR spectroscopy is more sensitive and informative with respect to local structural changes. Among a set of pulse EPR techniques, PDS EPR allows decoupling of the e-e d-d interactions in the electron spin echo signal, giving rise to a spin—spin distance distribution function $f(r)$ via an inversion of the dipolar trace [38,70]. Here, we exploit the Double Electron-Electron Resonance (DEER or PELDOR) experiments, since by such experiments, besides the $f(r)$ function, we can evaluate the mean number of spins N in the local aggregates [37,38], which is informative about possible peptide oligomerization upon metal ion binding. The DEER decay for a homogeneous distribution in the three-dimensional space is [38]:

$$V(T) = exp(-\alpha p_B CT)\cdot[1 - p_B<1 - (\cos(DT)>]^{N-1}. \quad (2)$$

The first term of the V(T) decay refers to the inter-molecular interaction, where α is $1.64\cdot10^{-12}$ cm^3/s [38], C is the spin probe concentration, and p_B is an excitation parameter, which is calculated from the EPR lineshape and the parameters of the excitation pulse (note that, for a given resonator on a model compound, the experimentally measured modulation depth λ is close to the calculated value ($\lambda_{exp}/\lambda_{calc} = 0.95$) [52]). The second term of the decay results from the intra-molecular interaction, where the function

$$\cos(DT) = \int_0^{\frac{\pi}{2}} \sin\theta d\theta \int_0^{\infty} \cos\left(\frac{g_A g_B \mu_B^2}{2\pi h r^3}\left(1 - 3\cos^2\theta\right)T\right) f(r)\, dr \quad (3)$$

is determined by averaging the pair distance distribution function $f(r)$. N is the number of spins in the local aggregate (for non-aggregated, double-labeled peptides, $N = 2$). The evaluation of the $f(r)$ function is an ill-posed problem and could be done via different approaches [60,70–72].

3.2. CW EPR Data

The continuous wave (cw) EPR spectra obtained for the spin-labeled peptide Tri^{1,8} with or without Ca(II) ions, at room temperature and at 100 K, are given in Figure 2a,b, respectively (results with other metal ions are given in Supplementary Information, Figure S1 and Table S1). At room temperature, the fast rotational tumbling regime averaged the electron Zeeman and hyperfine interactions to their isotropic values. The two nitroxides in Tri^{1,8} give a spectrum with three lines (parameters of the best fit are given in Supplementary Information, Table S1). The spectral values are close to those of a monoradical species, but with a bit of extra line broadening (the peak-to-peak width of the central transition is 0.35 mT, while for mono-labeled trichogins, values of 0.26–0.33 mT were reported [44]). Previously, for Tri^{1,8} in a polar solvent, we found the TOAC^1-TOAC^8 distance to be above 1.5 nm [24]. Therefore, the broadening cannot be attributed to a through-space exchange

coupling. Likely, this is mainly caused by modulation of the intramolecular dipole–dipole interaction [44]. For the Cu(II) species, the quartet is poorly resolved (Figure 2c). Notably, at room temperature, cw EPR spectra of both nitroxides and Cu(II) ions are insensitive to the possible interaction between metal ion and peptide, due to the fast motional tumbling, which results in averaging of electron–nuclei and electron–electron dipole-dipole interactions. In the frozen state, spectra show anisotropic structures, with inhomogeneously broadened lines. In the frozen state, spectra of nitroxides with or without metal ions are almost indistinguishable, with subtle changes on single linewidths after metal ion addition: a slight decrease for sodium and calcium can be seen, a small increase for copper (Figure 2b, Table S1). A salt effect of ions in the solution can be hypothesized. On the other hand, since the differences are small, this observation might derive from the absence of peptide–ion interactions, or from the fact that the change in the EPR fine structure is too subtle to be detected or it is hidden under inhomogeneous line broadening. A similar result is obtained when copper is observed with or without peptide (both *g*- and *A*-tensors do not change; Figure 2d, Table S1), but for the line broadening detected in the presence of the peptide. This broadening might be caused by changes of both *g*- and *A*-strains of the copper species, in turn due to modifications in the local surroundings, and indicates that such a type of coordination is rather weak.

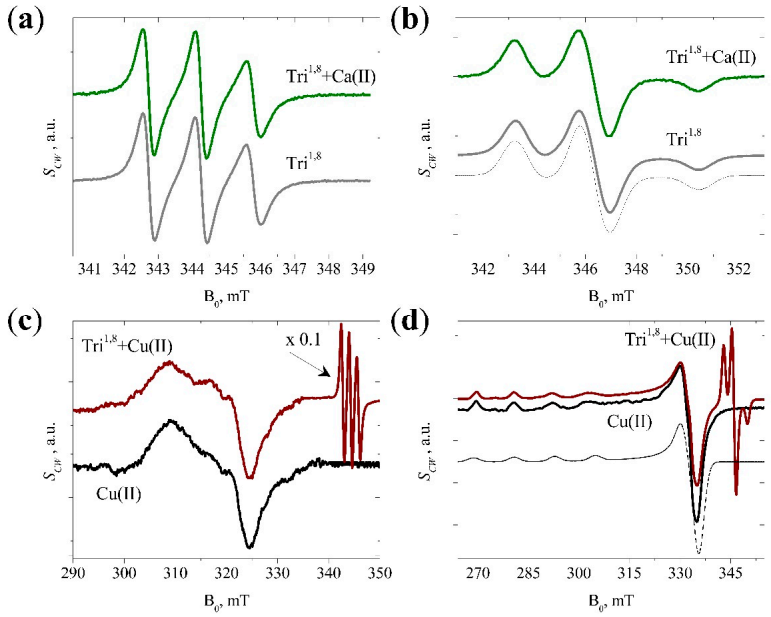

Figure 2. Continuous wave EPR spectra at room temperature (**a**,**c**) and at 100 K (**b**,**d**) for the double-labeled peptide Trichogin ($Tri^{1,8}$) alone and with calcium ($Tri^{1,8}$+Ca(II)) (**a**,**b**), and for Cu(II) species alone and with double-labeled peptide (**c**,**d**). Experimental data are shown by solid lines, while dashed lines are simulations for $Tri^{1,8}$, and Cu(II), respectively.

3.3. Pulse EPR Data

The normalized *intra*-molecular term of the DEER trace for double-labeled trichogin without ($Tri^{1,8}$) or with sodium, calcium, or copper ions [$Tri^{1,8}$+Na(I), $Tri^{1,8}$+Ca(II), $Tri^{1,8}$+Cu(II)] are shown by circles in Figure 3a (primary DEER decays and the cosine-Fourier images of the normalized traces are given in Supplementary Materials, Figure S3a,b). The most pronounced changes are detected with Ca(II) ions: the first minimum of dipolar oscillations shifts to longer times, and oscillations become more pronounced. With Na(I) ions, the oscillations even become obscured. An elongation of the dipolar frequency can be proposed with Cu(II) ions, without enhancement of the intensity of the dipolar oscillations. Since the oscillation frequency is determined by the mean spin–spin distance [37,54,69], and the oscillation intensity is determined by the dispersion of this distribution [38,44], the observed changes in the time domain point to structural modifications of the peptide helix in the presence of

either divalent ion. With Ca(II), we find an elongation of TOAC-TOAC distance, with a decrease in the dispersion of the distances. With Cu(II) species, some increase in the dipolar modulation period can be supposed, which points to elongation of TOAC-TOAC distances (Figure 3b).

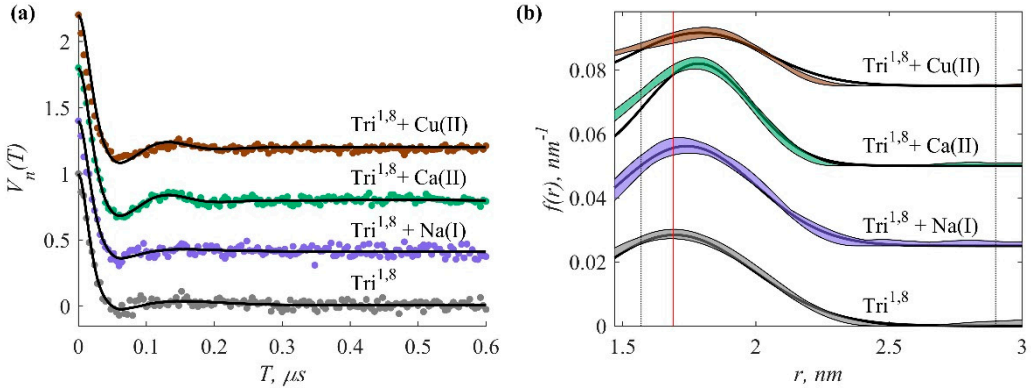

Figure 3. (**a**) Normalized DEER traces for Tri^{1,8} with or without metal ions. Colored circles, experimental data; black curves, the best fit. Traces are shifted up for clarity. (**b**) Distance distribution functions between spin labels in the peptide with or without metal ions, evaluated by DeerAnalysis (shaded areas show the confidence interval derived from data validation. Parameters and their variation boundaries are reported in paragraph 2.3), and its fit by an unimodal Gaussian distribution (black curves). Vertical, dashed lines limit the distance range unperturbed by truncation and sampling noises; the red line is at the mean TOAC-TOAC distance for Tri^{1,8} without metal ions. Distributions are shifted up for clarity. Color code of the systems is the same in both panels.

There are two possible reasons why the changes in the dipolar signals in the time-domain are so weak: (i) the intrinsic, short length of the peptide trichogin results in TOAC-TOAC distances close to the lower limit of the DEER method resolution [54,56,58]; (ii) the relatively small ion-induced distance change, in respect to the original TOAC-TOAC distance. In any case, such subtle changes need to be carefully validated. To this aim, the distance distribution functions were recovered both via a multi-Gaussian Monte Carlo approach [60] and by the model-free Tikhonov-based approach [70]. Both methods converged consistently for the tested distributions, with a small difference in the width of the distributions (Figure 2b, Table 1).

Table 1. Parameters of the Gaussian distribution between spin labels ($f(r) = 1/(\sqrt{2\pi\delta r^2})\cdot exp(-(r - <r>)^2/2\delta r^2)$, with related standard deviations. $<r>$, mean distance between labels; δr, dispersion of the related distribution.

Sample	$<r>$ ± Standard Deviation, nm	δr ± Standard Deviation, nm
Tri^{1,8}	1.695 [a] 1.69 ± 0.02 [b]	0.296 [a] 0.25 ± 0.03 [b]
Tri^{1,8} + Na(I)	1.74 [a] 1.72 ± 0.02 [b]	0.26 [a] 0.25 ± 0.02 [b]
Tri^{1,8} + Ca(II)	1.785 [a] 1.81 ± v0.02 [b]	0.2 [a] 0.17 ± 0.02 [b]
Tri^{1,8} + Cu(II)	1.79 [a] 1.78 ± 0.02 [b]	0.25 [a] 0.22 ± 0.02 [b]

[a] Evaluated by DeerAnalysis software. [b] Evaluated by the Multi-Gaussian Monte Carlo approach.

For trichogin without ions, the mean spin–spin distance is 1.69 nm, which points to the possible presence of an equilibrium between 3_{10}- and 2.2_7-helices, as already hypothesized in previous studies [24,44]. This TOAC^1-TOAC^8 distance of 1.69 nm in methanol solution agrees with literature FRET data recorded for the Fmoc^0-TOAC^8 analog of trichogin (Fmoc—fluorenylmethyloxycarbonyl), where the distance between Fmoc and TOAC^8 was

determined to be in the 1.39–1.45 nm range [33,49]. Indeed, the Fmoc group at the N-terminus is endowed with higher flexibility with respect to TOAC^{1} in the Tric^{1,8} analog. Therefore, Fmoc can get closer to TOAC^{8}, as compared to the immobilized nitroxide of TOAC^{1}. This possibility, in turn, accounts for the shorter distance observed by FRET in the Fmoc^{0}-TOAC^{8} analog. While the addition of Na(I) ions does not modify the spin–spin distance distribution function within the experimental error, for both Ca(II) and Cu(II) ions, a longer TOAC-TOAC distance is detected: the mean distance between spin labels is 1.05–1.07 and 1.05–1.06 times longer, respectively. In the case of the diamagnetic sodium ion, if the binding takes place without perturbing TOAC-TOAC distance, EPR would be unable to detect peptide–ion interactions. On the other hand, the consistency between the observed changes in pulse EPR data and the published results obtained by CD, FRET, and MD for trichogin-Na(I) [33], and for other peptide-Na(I) [25] systems seems to rule out significant trichogin-Na(I) interaction. Since the TOAC spin residue has a restricted conformational freedom [48], the dispersion of the spin–spin distribution is likely due to the inherent flexibility of the peptide chain. The short-length trichogin has been labeled at its N-terminus (TOAC^{1}), where the reduced H-bond pattern makes the residue a bit more flexible than the second label, located at the C-terminus (TOAC^{8}). Ion-driven changes in conformation flexibility, which causes a dispersion in the TOAC-TOAC distances, can give an indirect indication on the stability of peptide–ion complexes, and were also previously used for characterization of metal-binding properties in proteins of human, yeast, and bacterial families [46] A convenient way of measuring such conformation flexibility by EPR can be the determination of the ratio between distribution dispersion and the mean TOAC-TOAC distance (for an unimodal Gaussian distribution: $\delta r/r$). Applying this method to our data, we found that this ratio increases in the following order: Ca(II) < Cu(II) ≈ Na(I) ≈ peptide without ions. A narrower dispersion should point to stabilization of the peptide secondary structure, while a wider distance dispersion may arise from either a looser secondary structure, or the coexistence of several conformers with close spin–spin distances. We can conclude that trichogin binds to both calcium and copper ions, adapting its secondary structure, as already shown by previous studies, with each ion–peptide interaction probably driving different conformational changes in the peptide. It should be noted that for all samples, the intramolecular modulation depth is close to or lower than that expected for biradicals [69] (See Figure S2c). This is an indication that the interaction between trichogin and metal ions does not promote formation of peptide supramolecular structures. On the other hand, modulation depth reduction can also arise from alteration in the relative orientations of TOAC moieties; therefore we cannot tell whether the observed, ion-induced change in distance distribution is due to ion binding, as the literature suggests [33,34], or to the ions being able to create a distribution of peptide conformers. The short length of the peptide, which brings the spin–spin distance close to the lowest resolution limit of the technique [54,58], does not allow us to draw final conclusions on this observation. In the presence of Ca(II) ions, the peak at 1.69 nm is not observed. This means that all peptide molecules in solution are affected by ions, confirming a stoichiometric ratio of 1:1 between the metal ion and the peptide (the amount of peptide binding sites is 1), in agreement with previous studies [33].

To test the peptide binding efficiency, experiments varying peptide to metal ion ratios are typically performed [25]. In the case of pronounced differences, it is possible to effectively distinguish free peptide molecules from those bound to a metal ion. We tested Na(I) and Ca(II) ions because those ions gave the least and more pronounced spectral changes. Figure S4 reports a continuous wave EPR spectra acquired at different peptide to ion ratios. CW EPR was not able to detect differences in the lineshape at room temperature or at 100 K. Pulse DEER spectra for sodium ion at different peptide-to-ion ratios are also similar to those of Tri^{1,8} alone (Figure S5). The peptide/Ca(II) ratio 2:1 produced a distance distribution function in the form of a broad line centered at around 1.75 nm and the width of about 0.25 nm (Figure S5). This distribution cannot be fitted by Tri^{1,8} and Tri^{1,8}+Ca(II) alone, but might come from a superimposition of those two lines. However, due to overlapping of

functions, the deconvolution within the experimental accuracy is difficult and may lead to incorrect conclusions. We note that $f(r)$ undergoes similar changes in the presence of either Ca(II) (at peptide-to-ion ratio 2:1) or Cu(II) ions. Both the shift towards longer spin–spin distance and the line broadening seem to point to the onset of peptide–copper interactions. On the other hand, we cannot draw safe conclusions on the presence or absence of the peak at 1.69 nm. The broader distance distribution function observed in the case of peptide–Cu(II) interaction also complicates the deconvolution of the two lines at 1.69 and 1.78 nm, limiting the study of Cu-peptide systems at different peptide-to-ion ratios.

The structure of trichogin complexes with Ca(II) or Cu(II) ions is characterized by a longer distance between the two spin labels, in respect to the peptide alone, which can be explained by two different models. In the first model, the increase in the spin–spin distance is caused by a transition from a compact to a more extended helix. In such a model, the possible coordination of the metal ion occurs via the main peptide chain (through O and N atoms of the peptide bond), or via side chains. This second option is unlikely to occur in trichogin since its residues do not possess coordinating atoms in their side chains. Therefore, only the main chain is probably involved. In this connection, it is also worth considering a bidentate coordination from neighboring oxygens of the backbone. To further consider conformational implications, we created a model of $Tri^{1,8}$ in the 3_{10}-helical structure using Avogadro software [73]. The O-O distance between two neighboring carbonyl groups in that model is about 3.9 Å, which is large enough for Na(I) and Ca(II) coordination and for Cu(II) axial coordination [39]. As follows from Table 1, the mean distance between spin labels increases to about 0.9–1.2 Å in the presence of divalent ions. This value is less than the translation per amino acid of a α-helix (1.5 Å). If we roughly assume the peptide structure to be a mixture of just two helix types (3_{10} and 2.2_7), the observed change in the mean spin–spin distance would increase by a shift in the 'transition point' between the two helices by only one amino acid residue [16,26]). Thus, neither a subtle change in the type of helix nor a possible bidentate coordination of metal ions by the main peptide chain are enough to explain the observed peptide selectivity towards ions.

In the second model, we hypothesize that the peptide wraps around the ion, providing a more stable hairpin structure, as already described in previous experimental studies [33,34]. In this model, the coordination of the metal ion still takes place via the main-chain oxygens, but it is now stabilized by a multidentate coordination from the loop-motif (Figure 4).

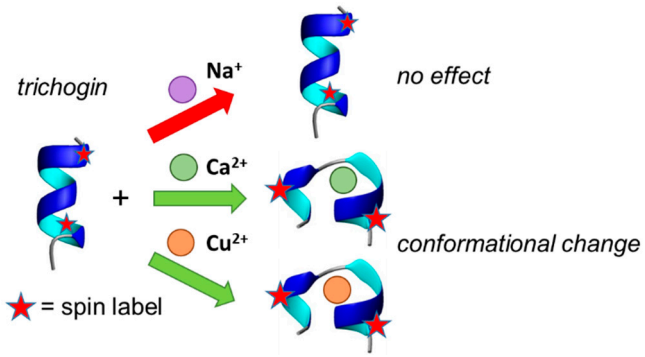

Figure 4. Schematic models built from literature data [33,34] and calculations [73] for ion–peptide interactions, explaining the longer distance between the two spin labels in the presence of Ca(II) or Cu(II) ions, in respect to the peptide alone, or with Na(I).

The second model apparently does not explain why trichogin seems to have different responses to certain ions. In FRET studies [33,34], a bimodal structure for trichogin-Ca(II) and trichogin-Gd(III) complexes was proposed, with a population of the dominant structure of about 85% for Ca(II) and 60% for Gd(III). The difference in the $f(r)$ dispersion described in the present work for Ca(II) and Cu(II) also seems to imply one preferable coordination state for Ca(II), while for Cu(II), several close conformers seem to be present. The difference

between Ca(II), Cu(II), and Gd(III) ions might be tentatively ascribed to the different ionic radii (effective ionic radii $r_{Ca(II)}$~1.0 Å, $r_{Cu(II)}$~0.65 Å, $r_{Gd(III)}$~0.938 Å [74]). Indeed, under this hypothesis, the relatively large hairpin of trichogin might result in a looser coordination shell for the small copper and gadolinium ions, while better fitting the larger Ca(II) ions. In addition, the main-chain carbonyl oxygen as a donor is common with calcium, but uncommon with other divalent metals [75,76]. It seems, however, that the ionic radius is not the pivotal parameter for coordination of the metal ion, since in both FRET and EPR studies, no binding was detected by trichogin to sodium ions, which has an effective ionic radius of $r_{Na(I)}$~1.02 Å [74] and is known to be less prone than Ca(II) to coordination via the main-chain carbonyl oxygens [77]. In addition, the coordination number (CN) seems to not be crucial in the selectivity towards metal ions, since for Cu(II), the CN is 4–6; for Ca(II) in proteins, it is 6–8; and for Na(I), it is 5–6 [74,76,78]. On the other hand, the hypothesis of the valence state could play a role. While the ionic radii are similar, the charge density for the divalent calcium (2.02 q/Å) is two times higher than that for the monovalent sodium ion. Therefore, a similar length of the metal-ligand bond should correspond to a larger bond strength for the Ca(II) species [79].

Finally, we believe metal ions can be exploited to shape and guide the formation of trichogin-based helical bundles. Indeed, it was reported that trichogin can favor transport of monovalent cations [Na(I), K(I)] across phospholipid membranes [80]. It was suggested that this process occurs via peptide oligomerization. Apparently, trichogin aggregation promotes the formation of a 'pocket', where sodium or potassium ions can be accommodated [43,80]. Such supramolecular structures could provide a more stable environment for coordinating monovalentions.

4. Conclusions

In summary, we demonstrated that EPR is a suitable technique to follow structural changes occurring in short, helical peptides such as trichogin in the presence of metal ions. The spin–spin distance in the double-labeled trichogin analog changes in response to the presence of divalent cations (calcium and copper), while it seems to not be affected by the presence of monovalent sodium ions. As shown in previous studies and discussed here, trichogin likely forms a loop in the presence of multivalent cations, which seems more efficient in catching Ca(II), rather than the Cu(II) species. We observed a stoichiometric ratio of 1:1 between the metal ion Ca(II) and the peptide, in agreement with previous studies.

The structural switch of the peptide and its selectivity to metal ions open new ways for exploiting peptides in advanced materials, either alone or linked to surfaces and nanoparticles. We believe that trichogin selectivity for certain ions, as well as its binding ratio and efficiency, can be triggered by appropriate modifications on its sequence, or by increasing the peptide length (e.g., by synthesizing trichogin dimers [25,43]).

Supplementary Materials: The following supporting information can be downloaded at: https://www.mdpi.com/article/10.3390/chemosensors10020071/s1, Figures S1–S5; Table S1.

Author Contributions: Conceptualization, M.D.Z. and V.N.S.; methodology, V.N.S.; software, V.N.S.; validation, M.D.Z., V.N.S. and F.F.; formal analysis, V.N.S.; investigation, V.N.S. and A.S.S.; resources, M.D.Z., V.N.S. and F.F.; data curation, V.N.S.; writing—original draft preparation, V.N.S.; writing—review and editing, M.D.Z., V.N.S. and F.F.; supervision, M.D.Z. and V.N.S.; funding acquisition, M.D.Z., F.F. and V.N.S. All authors have read and agreed to the published version of the manuscript.

Funding: This research was funded by the Russian Science Foundation (project #21-13-00025), Centro Studi "Giorgio Levi Cases", the Italian Ministry for University and Research (MUR) (PRIN Projects 20173LBZM2 and 2020833Y75), and the University of Padova (Project P-DiSC#04BIRD2019-UNIPD).

Institutional Review Board Statement: Not applicable.

Informed Consent Statement: Not applicable.

Data Availability Statement: The data are available by authors by request.

Acknowledgments: The authors are thankful to Ekaterina F. Afanasyeva for preliminary EPR measurements.

Conflicts of Interest: The authors declare no conflict of interest. The funders had no role in the design of the study; in the collection, analyses, or interpretation of data; in the writing of the manuscript, or in the decision to publish the results.

References

1. Zasloff, M. Antimicrobial peptides of multicellular organisms. *Nature* **2002**, *415*, 389–395. [CrossRef]
2. Bechinger, B.; Lohner, K. Detergent-like actions of linear amphipathic cationic antimicrobial peptides. *Biochim. Biophys. Acta BBA Biomembr.* **2006**, *1758*, 1529–1539. [CrossRef]
3. Jenssen, H.; Hamill, P.; Hancock, R.E. Peptide antimicrobial agents. *Clin. Microbiol. Rev.* **2006**, *19*, 491–511. [CrossRef]
4. Ashkenasy, G.; Ghadiri, M.R. Boolean logic functions of a synthetic peptide network. *J. Am. Chem. Soc.* **2004**, *126*, 11140–11141. [CrossRef]
5. Mejáre, M.; Bülow, L. Metal-binding proteins and peptides in bioremediation and phytoremediation of heavy metals. *Trends Biotechnol.* **2001**, *19*, 67–73. [CrossRef]
6. Chow, E.; Gooding, J.J. Peptide modified electrodes as electrochemical metal ion sensors. *Electroanalysis* **2006**, *18*, 1437–1448. [CrossRef]
7. Knerr, P.J.; Branco, M.C.; Nagarkar, R.; Pochan, D.J.; Schneider, J.P. Heavy metal ion hydrogelation of a self-assembling peptide via cysteinyl chelation. *J. Mater. Chem.* **2012**, *22*, 1352–1357. [CrossRef]
8. Zegota, M.M.; Müller, M.A.; Lantzberg, B.; Kizilsavas, G.; Coelho, J.A.S.; Moscariello, P.; Martínez-Negro, M.; Morsbach, S.; Gois, P.M.P.; Wagner, M.; et al. Dual Stimuli-Responsive Dynamic Covalent Peptide Tags: Toward Sequence-Controlled Release in Tumor-like Microenvironments. *J. Am. Chem. Soc.* **2021**, *143*, 17047–17058. [CrossRef]
9. Löwik, D.W.P.M.; Leunissen, E.H.P.; van den Heuvel, M.; Hansen, M.B.; van Hest, J.C.M. Stimulus responsive peptide based materials. *Chem. Soc. Rev.* **2010**, *39*, 3394–3412. [CrossRef] [PubMed]
10. Tertis, M.; Hosu, O.; Feier, B.; Cernat, A.; Florea, A.; Cristea, C. Electrochemical Peptide-Based Sensors for Foodborne Pathogens Detection. *Molecules* **2021**, *26*, 3200. [CrossRef]
11. Ronda, L.; Tonelli, A.; Sogne, E.; Autiero, I.; Spyrakis, F.; Pellegrino, S.; Abbiati, G.; Maffioli, E.; Schulte, C.; Piano, R.; et al. Rational Design of a User-Friendly Aptamer/Peptide-Based Device for the Detection of *Staphylococcus aureus*. *Sensors* **2020**, *20*, 4977. [CrossRef]
12. Shah, A.; Malik, M.S.; Khan, G.S.; Nosheen, E.; Iftikhar, F.J.; Khan, F.A.; Shukla, S.S.; Akhter, M.S.; Kraatz, H.-B.; Aminabhavi, T.M. Stimuli-responsive peptide-based biomaterials as drug delivery systems. *Chem. Eng. J.* **2018**, *353*, 559–583. [CrossRef]
13. Mart, R.J.; Osborne, R.D.; Stevens, M.M.; Ulijn, R.V. Peptide-based stimuli-responsive biomaterials. *Soft Matter* **2006**, *2*, 822–835. [CrossRef]
14. Liu, G.; Lovell, J.F.; Zhang, L.; Zhang, Y. Stimulus-Responsive Nanomedicines for Disease Diagnosis and Treatment. *Int. J. Mol. Sci.* **2020**, *21*, 6380. [CrossRef]
15. Lee, D.; Rejinold, N.S.; Jeong, S.D.; Kim, Y.-C. Stimuli-Responsive Polypeptides for Biomedical Applications. *Polymers* **2018**, *10*, 830. [CrossRef]
16. La Manna, S.; Di Natale, C.; Onesto, V.; Marasco, D. Self-Assembling Peptides: From Design to Biomedical Applications. *Int. J. Mol. Sci.* **2021**, *22*, 12662. [CrossRef]
17. Arul, A.; Sivagnanam, S.; Dey, A.; Mukherjee, O.; Ghosh, S.; Das, P. The design and development of short peptide-based novel smart materials to prevent fouling by the formation of non-toxic and biocompatible coatings. *RSC Adv.* **2020**, *10*, 13420–13429. [CrossRef]
18. Kubitzky, S.; Venanzi, M.; Biondi, B.; Lettieri, R.; De Zotti, M.; Gatto, E. A pH-Induced Reversible Conformational Switch Able to Control the Photocurrent Efficiency in a Peptide Supramolecular System. *Chem. Eur. J.* **2021**, *27*, 2810–2817. [CrossRef]
19. Cerpa, R.; Cohen, F.E.; Kuntz, I.D. Conformational switching in designed peptides: The helix/sheet transition. *Fold. Des.* **1996**, *1*, 91–101. [CrossRef]
20. Zuber, P.K.; Schweimer, K.; Rösch, P.; Artsimovitch, I.; Knauer, S.H. Reversible fold-switching controls the functional cycle of the antitermination factor RfaH. *Nat. Commun.* **2019**, *10*, 702. [CrossRef] [PubMed]
21. Selegård, R.; Aronsson, C.; Brommesson, C.; Dånmark, S.; Aili, D. Folding driven self-assembly of a stimuli-responsive peptide-hyaluronan hybrid hydrogel. *Sci. Rep.* **2017**, *7*, 7013. [CrossRef] [PubMed]
22. Mueller, C.; Grossmann, T.N. Coiled-Coil Peptide Beacon: A Tunable Conformational Switch for Protein Detection. *Angew. Chem. Int. Ed.* **2018**, *57*, 17079–17083. [CrossRef]
23. Chen, Y.; Cruz-Chu, E.R.; Woodard, J.C.; Gartia, M.R.; Schulten, K.; Liu, L. Electrically Induced Conformational Change of Peptides on Metallic Nanosurfaces. *ACS Nano* **2012**, *6*, 8847–8856. [CrossRef]
24. De Zotti, M.; Syryamina, V.N.; Hussain, R.; Longo, E.; Siligardi, G.; Dzuba, S.; Stella, L.; Formaggio, F. A Temperature-Driven, Reversible, Helical-Handedness Inversion in Peptaibol Analogues Tuned by the C-Terminal Capping Moiety. *ChemBioChem* **2019**, *20*, 2125–2132. [CrossRef] [PubMed]

25. Meron, S.; Shenberger, Y.; Ruthstein, S. The Advantages of EPR Spectroscopy in Exploring Diamagnetic Metal Ion Binding and Transfer Mechanisms in Biological Systems. *Magnetochemistry* **2022**, *8*, 3. [CrossRef]
26. Shults, M.D.; Pearce, D.A.; Imperiali, B. Modular and tunable chemosensor scaffold for divalent zinc. *J. Am. Chem. Soc.* **2003**, *125*, 10591–10597. [CrossRef] [PubMed]
27. Abu-Ali, H.; Nabok, A.; Smith, T.J. Development of novel and highly specific ssDNA-aptamer-based electrochemical biosensor for rapid detection of mercury (II) and lead (II) ions in water. *Chemosensors* **2019**, *7*, 27. [CrossRef]
28. Coskun, A.; Deniz, E.; Akkaya, E.U. Effective PET and ICT switching of boradiazaindacene emission: A unimolecular, emission-mode, molecular half-subtractor with reconfigurable logic gates. *Org. Lett.* **2005**, *7*, 5187–5189. [CrossRef]
29. Zou, R.; Wang, Q.; Wu, J.; Wu, J.; Schmuck, C.; Tian, H. Peptide self-assembly triggered by metal ions. *Chem. Soc. Rev.* **2015**, *44*, 5200–5219. [CrossRef]
30. Johnson, R.A.; Manley, O.M.; Spuches, A.M.; Grossoehme, N.E. Dissecting ITC data of metal ions binding to ligands and proteins. *Biochim. Biophys. Acta Gen. Subj.* **2016**, *1860*, 892–901. [CrossRef]
31. Dawson, W.M.; Lang, E.J.M.; Rhys, G.G.; Shelley, K.L.; Williams, C.; Brady, R.L.; Crump, M.P.; Mulholland, A.J.; Woolfson, D.N. Structural resolution of switchable states of a *de novo* peptide assembly. *Nat. Commun.* **2021**, *12*, 1530. [CrossRef]
32. Liu, Z.; Chen, S.; Qiao, F.; Zhang, X. Interaction of peptide backbones and transition metal ions: 1. an IM-MS and DFT study of the binding pattern, structure and fragmentation of Pd(II)/Ni(II)-Polyalanine complexes. *Int. J. Mass Spectrom.* **2019**, *438*, 87–96. [CrossRef]
33. Venanzi, M.; Bocchinfuso, G.; Gatto, E.; Palleschi, A.; Stella, L.; Formaggio, F.; Toniolo, C. Metal Binding Properties of Fluorescent Analogues of Trichogin GA IV: A Conformational Study by Time-Resolved Spectroscopy and Molecular Mechanics Investigations. *ChemBioChem* **2009**, *10*, 91–97. [CrossRef] [PubMed]
34. Gatto, E.; Palleschi, M.E.; Zangrilli, B.; De Zotti, M.; Di Napoli, B.; Palleschi, A.; Mazzuca, C.; Formaggio, F.; Toniolo, C.; Venanzi, M. The several facets of Trichogin GA IV: High affinity Tb (III) binding properties. A spectroscopic and molecular dynamics simulation study. *Pept. Sci.* **2018**, *110*, e24081. [CrossRef]
35. She, F.; Teng, P.; Peguero-Tejada, A.; Wang, M.; Ma, N.; Odom, T.; Zhou, M.; Gjonaj, E.; Wojtas, L.; van der Vaart, A.; et al. De Novo Left-Handed Synthetic Peptidomimetic Foldamers. *Angew. Chem.* **2018**, *130*, 10064–10068. [CrossRef]
36. Worswick, S.G.; Spencer, J.A.; Jeschke, G.; Kuprov, I. Deep neural network processing of DEER data. *Sci. Adv.* **2018**, *4*, eaat5218. [CrossRef]
37. Milov, A.D.; Salikhov, K.M.; Shirov, M.D. Application of ELDOR in electron-spin echo for paramagnetic center space distribution in solids. *Fizika Tverdogo Tela* **1981**, *23*, 975–982.
38. Milov, A.D.; Maryasov, A.G.; Tsvetkov, Y.D. Pulsed electron double resonance (PELDOR) and its applications in free-radicals research. *Appl. Magn. Reson.* **1998**, *15*, 107–143. [CrossRef]
39. Jeschke, G. Determination of the nanostructure of polymer materials by electron paramagnetic resonance spectroscopy. *Macromol. Rapid Commun.* **2002**, *23*, 227–246. [CrossRef]
40. Millhauser, G.L. Selective placement of electron spin resonance spin labels: New structural methods for peptides and proteins. *Trends Biochem. Sci.* **1992**, *17*, 448–452. [CrossRef]
41. Hubbell, W.L.; Altenbach, C. Investigation of structure and dynamics in membrane proteins using site-directed spin labeling. *Curr. Opin. Struct. Biol.* **1994**, *4*, 566–573. [CrossRef]
42. Tkach, I.; Diederichsen, U.; Bennati, M. Studies of transmembrane peptides by pulse dipolar spectroscopy with semi-rigid TOPP spin labels. *Eur. Biophys. J.* **2021**, *50*, 143–157. [CrossRef] [PubMed]
43. Chiang, Y.-W.; Borbat, P.P.; Freed, J.H. The determination of pair distance distributions by pulsed ESR using Tikhonov regularization. *J. Magn. Reson.* **2005**, *172*, 279–295. [CrossRef]
44. Milov, A.D.; Tsvetkov, Y.D.; Raap, J.; De Zotti, M.; Formaggio, F.; Toniolo, C. Conformation, self-aggregation, and membrane interaction of peptaibols as studied by pulsed electron double resonance spectroscopy. *Pept. Sci.* **2016**, *106*, 6–24. [CrossRef]
45. Faller, P.; Hureau, C.; Dorlet, P.; Hellwig, P.; Coppel, Y.; Collin, F.; Alies, B. Methods and techniques to study the bioinorganic chemistry of metal–peptide complexes linked to neurodegenerative diseases. *Coord. Chem. Rev.* **2012**, *256*, 2381–2396. [CrossRef]
46. Shenberger, Y.; Gottlieb, H.E.; Ruthstein, S. EPR and NMR spectroscopies provide input on the coordination of Cu (I) and Ag (I) to a disordered methionine segment. *JBIC J. Biol. Inorg. Chem.* **2015**, *20*, 719–727. [CrossRef]
47. Shenberger, Y.; Yarmiayev, V.; Ruthstein, S. Exploring the interaction between the human copper transporter, CTR1, c-terminal domain and a methionine motif in the presence of Cu (I) and Ag (I) ions, using EPR spectroscopy. *Mol. Phys.* **2013**, *111*, 2980–2991. [CrossRef]
48. Biondi, B.; Syryamina, V.; Rocchio, G.; Barbon, A.; Formaggio, F.; Toniolo, C.; Raap, J.; Dzuba, S.A. Is Cys(MTSL) the Best α-Amino Acid Residue to Electron Spin Labeling Helical Peptide Molecules? *ACS Omega* **2022**. [CrossRef]
49. Venanzi, M.; Gatto, E.; Bocchinfuso, G.; Palleschi, A.; Stella, L.; Formaggio, F.; Toniolo, C. Dynamics of Formation of a Helix–Turn–Helix Structure in a Membrane-Active Peptide: A Time-Resolved Spectroscopic Study. *ChemBioChem* **2006**, *7*, 43–45. [CrossRef] [PubMed]
50. De Zotti, M.; Biondi, B.; Peggion, C.; Formaggio, F.; Park, Y.; Hahm, K.S.; Toniolo, C. Trichogin GA IV: A versatile template for the synthesis of novel peptaibiotics. *Org. Biomol. Chem.* **2012**, *10*, 1285–1299. [CrossRef]

51. De Zotti, M.; Sella, L.; Bolzonello, A.; Gabbatore, L.; Peggion, C.; Bortolotto, A.; Elmaghraby, I.; Tundo, S.; Favaron, F. Targeted Amino Acid Substitutions in a Trichoderma Peptaibol Confer Activity against Fungal Plant Pathogens and Protect Host Tissues from Botrytis cinerea Infection. *Int. J. Mol. Sci.* **2020**, *21*, 7521. [CrossRef]
52. Syryamina, V.N.; Matveeva, A.G.; Vasiliev, Y.V.; Savitsky, A.; Grishin, Y.A. Improving B1 field homogeneity in dielectric tube resonators for EPR spectroscopy via controlled shaping of the dielectric insert. *J. Magn. Reson.* **2020**, *311*, 106685. [CrossRef]
53. Matveeva, A.G.; Syryamina, V.N.; Nekrasov, V.M.; Bowman, M.K. Non-uniform sampling in pulse dipolar spectroscopy by EPR: The redistribution of noise and the optimization of data acquisition. *Phys. Chem. Chem. Phys.* **2021**, *23*, 10335–10346. [CrossRef] [PubMed]
54. Tsvetkov, Y.D.; Milov, A.D.; Maryasov, A.G. Pulsed electron–electron double resonance (PELDOR) as EPR spectroscopy in nanometre range. *Russ. Chem. Rev.* **2008**, *77*, 487. [CrossRef]
55. Milov, A.D.; Grishin, Y.A.; Dzuba, S.A.; Tsvetkov, Y.D. Effect of pumping pulse duration on echo signal amplitude in Four-Pulse PELDOR. *Appl. Magn. Reson.* **2011**, *41*, 59–67. [CrossRef]
56. Jeschke, G.; Polyhach, Y. Distance measurements on spin-labeled biomacromolecules by pulsed electron paramagnetic resonance. *Phys. Chem. Chem. Phys.* **2007**, *9*, 1895–1910. [CrossRef]
57. Fajer, P.G.; Brown, L.; Song, L. Practical pulsed dipolar ESR (DEER). In *ESR Spectroscopy in Membrane Biophysics*; Springer: Boston, MA, USA, 2007; pp. 95–128.
58. Schiemann, O.; Heubach, C.A.; Abdullin, D.; Ackermann, K.; Azarkh, M.; Bagryanskaya, E.G.; Drescher, M.; Endeward, B.; Freed, J.H.; Galazzo, L.; et al. Benchmark test and guidelines for DEER/PELDOR experiments on nitroxide-labeled biomolecules. *J. Am. Chem. Soc.* **2021**, *143*, 17875–17890. [CrossRef] [PubMed]
59. Stoll, S.; Schweiger, A. EasySpin, a comprehensive software package for spectral simulation and analysis in EPR. *J. Magn. Reson.* **2006**, *178*, 42–55. [CrossRef]
60. Matveeva, A.G.; Yushkova, Y.V.; Morozov, S.V.; Grygor'ev, I.A.; Dzuba, S.A. Multi-Gaussian Monte Carlo analysis of PELDOR data in the frequency domain. *Zeitschrift für Physikalische Chemie* **2017**, *231*, 671–688. [CrossRef]
61. Pannier, M.; Schädler, V.; Schöps, M.; Wiesner, U.; Jeschke, G.; Spiess, H.W. Determination of ion cluster sizes and cluster-to-cluster distances in ionomers by four-pulse double electron electron resonance spectroscopy. *Macromolecules* **2000**, *33*, 7812–7818. [CrossRef]
62. Jeschke, G.; Chechik, V.; Ionita, P.; Godt, A.; Zimmermann, H.; Banham, J.; Timmel, C.R.; Hilger, D.; Jung, H. DeerAnalysis2006—A comprehensive software package for analyzing pulsed ELDOR data. *Appl. Magn. Reson.* **2006**, *30*, 473–498. [CrossRef]
63. Brandon, S.; Beth, A.H.; Hustedt, E.J. The global analysis of DEER data. *J. Magn. Reson.* **2012**, *218*, 93–104. [CrossRef]
64. Syryamina, V.N.; De Zotti, M.; Toniolo, C.; Formaggio, F.; Dzuba, S.A. Alamethicin self-assembling in lipid membranes: Concentration dependence from pulsed EPR of spin labels. *Phys. Chem. Chem. Phys.* **2018**, *20*, 3592–3601. [CrossRef]
65. Kuznetsova, A.A.; Matveeva, A.G.; Milov, A.D.; Vorobjev, Y.N.; Dzuba, S.A.; Fedorova, O.S.; Kuznetsov, N.A. Substrate specificity of human apurinic/apyrimidinic endonuclease APE1 in the nucleotide incision repair pathway. *Nucleic Acids Res.* **2018**, *46*, 11454–11465. [CrossRef] [PubMed]
66. Edwards, T.H.; Stoll, S. A Bayesian approach to quantifying uncertainty from experimental noise in DEER spectroscopy. *J. Magn. Reson.* **2016**, *270*, 87–97. [CrossRef] [PubMed]
67. Peisach, J.; Blumberg, W.E. Structural implications derived from the analysis of electron paramagnetic resonance spectra of natural and artificial copper proteins. *Arch. Biochem. Biophys.* **1974**, *165*, 691–708. [CrossRef]
68. Abdullin, D.; Schiemann, O. Pulsed Dipolar EPR Spectroscopy and Metal Ions: Methodology and Biological Applications. *ChemPlusChem* **2020**, *85*, 353–372. [CrossRef]
69. Salikhov, K.M.; Khairuzhdinov, I.T.; Zaripov, R.B. Three-pulse ELDOR theory revisited. *Appl. Magn. Reson.* **2014**, *45*, 573–619. [CrossRef]
70. Jeschke, G.; Panek, G.; Godt, A.; Bender, A.; Paulsen, H. Data analysis procedures for pulse ELDOR measurements of broad distance distributions. *Appl. Magn. Reson.* **2004**, *26*, 223–244. [CrossRef]
71. Chiang, Y.W.; Borbat, P.P.; Freed, J.H. Maximum entropy: A complement to Tikhonov regularization for determination of pair distance distributions by pulsed ESR. *J. Magn. Reson.* **2005**, *177*, 184–196. [CrossRef] [PubMed]
72. Dzuba, S.A. The determination of pair-distance distribution by double electron–electron resonance: Regularization by the length of distance discretization with Monte Carlo calculations. *J. Magn. Reson.* **2016**, *269*, 113–119. [CrossRef] [PubMed]
73. Open Source. Avogadro. Available online: https://avogadro.cc/ (accessed on 10 January 2022).
74. Figgis, B.N.; Hitchman, M.A. *Ligand Field Theory and Its Applications*; Wiley-Vch: New York, NY, USA, 2000; p. 158.
75. Shannon, R.D. Revised effective ionic radii and systematic studies of interatomic distances in halides and chalcogenides. *Acta Crystallogr. Sect. A Cryst. Phys. Diffr. Theor. Gen. Crystallogr.* **1976**, *32*, 751–767. [CrossRef]
76. Harding, M.M. Geometry of metal–ligand interactions in proteins. *Acta Crystallogr. Sect. D Biol. Crystallogr.* **2001**, *57*, 401–411. [CrossRef]
77. Harding, M.M. The architecture of metal coordination groups in proteins. *Acta Crystallogr. Sect. D Biol. Crystallogr.* **2004**, *60*, 849–859. [CrossRef]
78. Harding, M.M. Metal–ligand geometry relevant to proteins and in proteins: Sodium and potassium. *Acta Crystallogr. Sect. D Biol. Crystallogr.* **2002**, *58*, 872–874. [CrossRef] [PubMed]

79. Dudev, T.; Lim, C. Competition among metal ions for protein binding sites: Determinants of metal ion selectivity in proteins. *Chem. Rev.* **2014**, *114*, 538–556. [CrossRef]
80. Kropacheva, T.N.; Raap, J. Ion transport across a phospholipid membrane mediated by the peptide trichogin GA IV. *Biochim. Biophys. Acta BBA Biomembr.* **2002**, *1567*, 193–203. [CrossRef]